# UPGRADE OF THE EXTERNAL BEAMLINE AT THE MICROANALYTICAL CENTER OF THE JOŽEF STEFAN INSTITUTE

K. Isaković[1,*], M. Petric[2,3], Z. Rupnik[2], Ž. Šmit[2,4], P. Pelicon[2], M. Kelemen[1,2], M. Vereš[2], P. Pongrac[2,5], P. Vavpetič[2] and M. Kavčič[2,4,*]

[1]*Jožef Stefan International Postgraduate School, Jamova 39, 1000 Ljubljana, Slovenia.*

[2]*Jožef Stefan Institute, Jamova 39, SI-1000 Ljubljana, Slovenia.*

[3]*Faculty of Geotechnical Engineering, University of Zagreb, Hallerova aleja 7, 42000 Varaždin, Croatia.*

[4]*Faculty of Mathematics and Physics, University of Ljubljana, Jadranska 19, 1000 Ljubljana, Slovenia*

[5] *Biotechnical Faculty, University of Ljubljana, Jamnikarjeva 101, 1000 Ljubljana, Slovenia*

## HIGHLIGHTS:

- Our external beamline has been upgraded to achieve beam focusing and provide in-air PIXE imaging.
- Lateral resolution of 50 μm was achieved using magnetic quadrupole lenses and ultrathin $Si_3N_4$ exit window.
- Quantitative concentration maps of a longitudinal section of a whole thick wheat grain have been determined.

ABSTRACT

The existing external beamline at the Microanalytical Center of the Jožef Stefan Institute (JSI) in Ljubljana has been currently upgraded in order to extend the capabilities towards in-air PIXE imaging across relatively large sample surface area (~ 1 $cm^2$) with lateral resolution of sub 100 μm. For that purpose, a doublet of magnetic quadrupole lenses was installed on the beamline together with the newly designed exit nozzle with a 200 nm $Si_3N_4$ exit window resulting finally in ~ 50×50 $\mu m^2$ lateral resolution. Additionally, an in-vacuum beam chopper was installed before the exit nozzle to measure the proton dose deposited on the sample. The beam characterization results are presented together with the first application from the field of biology, namely quantitative concentration maps of a longitudinal section of a whole thick wheat grain.

*Keywords*: External proton beam, PIXE analysis, concentration maps

## I. INTRODUCTION

Because of its high sensitivity, non-destructive character, and capability to perform full quantitative analysis, Particle Induced X-ray Emission (PIXE) technique is commonly used to analyze multi-elemental composition of the studied samples from various research disciplines. Using magnetic

* Corresponding authors:
kristina.isakovic@ijs.si
matjaz.kavcic@ijs.si

quadruple lenses, a MeV proton beam can be effectively focused down to ~ 1 μm$^2$ size and scanned across the sample using the scanning coils to record quantitative concentration maps with micrometer lateral resolution [1]. At the Microanalytical Center of the Jožef Stefan Institute (JSI) in Ljubljana hosting a 2 MV Tandem accelerator, micro-PIXE analysis is regularly performed at the microprobe beamline based on the triplet quadrupole lens system from Oxford Microbeams (OM-150) [1] and applied successfully to biomedical applications [2-4]. While in these applications we are usually looking for maximal lateral resolution and the size of the scanning area is usually of the order of mm$^2$ and lower, we have been recently faced with the requirements to increase significantly the scanning area to allow PIXE imaging of larger objects (few cm$^2$) at the expense of moderate sub 100 μm spatial resolution, which would complement detailed micro-PIXE analysis. For that purpose, we have decided to upgrade the external beamline which has been so far mainly used for in-air PIXE archaeometry studies employing point analysis with a broad (~ 1 mm) proton beam [5-8]. The main goal was to achieve in-air beam focusing down to few tens of μm, which would allow us to perform in-air PIXE analysis of larger biological objects with very little sample preparation.

The manuscript presents the main technical specifications of this upgrade and the results of characterization measurements providing actual experimental lateral resolution. Finally, the new setup is used to analyze a longitudinal section of a whole thick wheat grain illustrating the capabilities of this new setup for in-air PIXE imaging of large objects and surface areas with sub 100 μm lateral resolution.

## II. EXPERIMENTAL SETUP

The external proton beam is situated at the -30$^o$ exit port of switching magnet of the 2 MV Tandem ion accelerator. During the current upgrade the beamline was equipped with water-cooled object slits positioned at the beginning of the beamline after the switching magnet. Next, a second set of collimator slits was installed further down in front of the quadrupole doublet (manufactured by Drusch et Cie), which is used to focus the beam on the target. The distance between the object slits and quadrupole doublet is 550 cm while the distance between the quadrupole doublet and the exit window is 74 cm. Before the exit nozzle an in-beam chopper device [9,10] has been installed. The rotating chopper (gold plated carbon blades) periodically intersects the beam in vacuum just before it exits through the exit window into the ambient atmosphere. The spectrum of the backscattered protons is recorded simultaneously with the PIXE spectra and the integrated Au Rutherford Backscattering Spectrometry (RBS) peak is used to measure the proton dose, which serves for normalization. Finally, the exit nozzle terminating the beamline was redesigned to optimize the detection geometry and minimize the sample-exit window working distance. For this purpose, it accommodates a 3×3 mm$^2$ Si frame with an ultra-thin 200 nm $Si_3N_4$ window necessary to diminish the lateral beam scattering in the foil. The redesigned exit nozzle also allows to use smaller exit window-sample distance, which is crucial for achieving good lateral resolution. The sample is placed on the motorized computer controlled XYZ stage (manufactured by ISEL automation), which is used to move and position the sample with steps of 12 μm. The relative

position of the beam on the sample window is adjusted using a microscope. The microscope is used also to adjust properly the sample distance from the exit window by positioning the sample into the focal plane of the microscope. The end station is equipped with two Si(Li) detectors for PIXE analysis positioned at 135° with respect to the primary beam direction. The Si(Li) detector (manufactured by PGT, active area 30 $mm^2$, 7.5 μm thin Be window, 138 eV FWHM resolution at 5.9 keV) positioned above the beam at a distance of 3.2 cm from the sample is used for in air PIXE imaging (label 1 in Figure 2) presented later on in the manuscript. The second PIXE detector (label 6 in Figure 2) was used previously for in-air PIXE archaeometry studies with a broad proton beam [5-8] and is in fact not applied in current imaging applications. Beside both PIXE detectors, the end station is equipped with an additional high-purity Ge detector (P-type coaxial manufactured by ORTEC) for Particle-Induced Gamma Emission (PIGE) analysis. The schematic layout of the beamline is presented in Figure 1 and the photograph of the exit nozzle and the detector configuration at the beamline end station is shown in Figure 2.

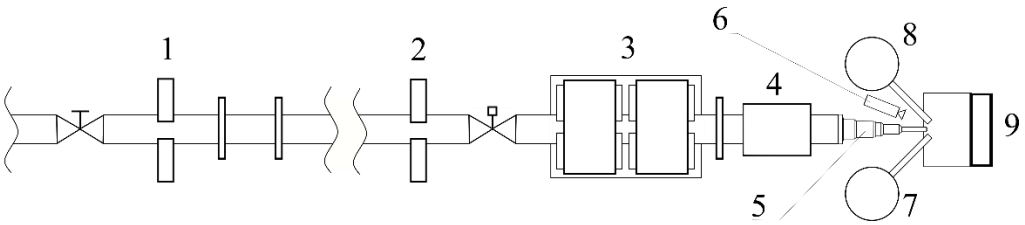


**Figure 1**: Schematic view of the upgraded beamline for in-air PIXE analysis at the Microanalytical center of the Jožef Stefan Institute. (1) water cooled object slits, (2) collimator slits, (3) quadrupole doublet, (4) in beamline chopper, (5) exit nozzle, (6) microscope, (7) Si(Li) X-ray detector, (8) HP Ge gamma detector, (9) XYZ motorized stage.

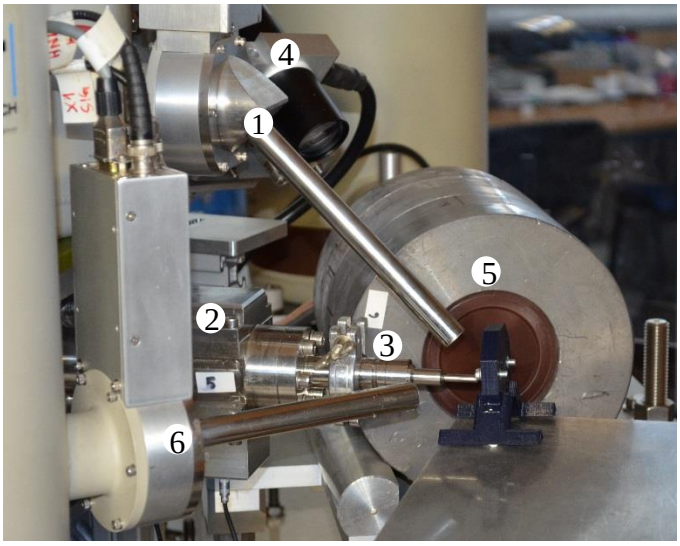


**Figure 2**: A photo of the upgraded external beam setup. (1) Si(Li) X-ray detector, (2) in beamline chopper, (3) exit nozzle, (4) microscope, (5) HP Ge gamma detector, (6) Si(Li) X-ray detector.

## III. CHARACTERIZATION RESULTS

The most important parameter we have first tried to quantify is the actual size of the proton beam spot on the sample. In order to achieve optimal focusing we have first inserted a scintillator in the proton beam and roughly adjusted the magnetic fields of both quadrupoles by observing the shape and size of the fluorescence spot under the microscope. After that, the beam size has been measured using the knife-edge method [11]. In this measurement a metallic blade is moved across the beam in 15 μm steps and the X-ray yield is recorded as a function of sample stage position. This is used to perform the fine tuning of the magnetic fields of both quadrupoles required to reach optimal focusing.

Besides the focusing capability of the quadrupole doublet the actual size of the beam on the target is defined by the lateral straggling of protons in their passage through the $Si_3N_4$ foil and the air gap between the exit window and the sample. The exit window and ambient atmosphere cause lateral and energy straggling of protons and, as it was reported in earlier studies [9,10,12], with thin silicon nitride windows the beam broadening is primarily caused by scattering in air while for thicker windows the most important effect is scattering in the foil. We calculated this effect by using the SRIM code showing the dependence of the beam size on the distance from the exit window. Since SRIM is a Monte Carlo simulation of an ensemble of individual protons from the same point such calculations do not take into account the finite size of the proton beam entering the exit window due to the limited focusing power of the quadrupole lenses. For that purpose, we have verified both effects by performing beam size characterization measurements as a function of the distance from the exit window. Results of these measurements are presented in Figure 3 together with the results of SRIM simulation. The measured dependence fits well to the model composed of SRIM simulation with an addition of linear curve representing the finite divergence of the proton beam leaving the exit window. In order to keep the lateral resolution in the sub 100 μm regime we need to position the sample relatively close to the exit nozzle at the distance below 7 mm. In order to illustrate the actual experimental lateral resolution we have performed PIXE mapping of a Platinum/Rhodium mesh (Pt90/Rh10) positioned at a working distance of 3 mm away from the exit window. The beam size (FWHM) determined from the knife-edge measurement at the same working distance used in the mapping was found 52 ± 5 μm (horizontal dimension) times 43 ± 3 μm (vertical dimension). The measured PIXE map is presented in Figure 4.

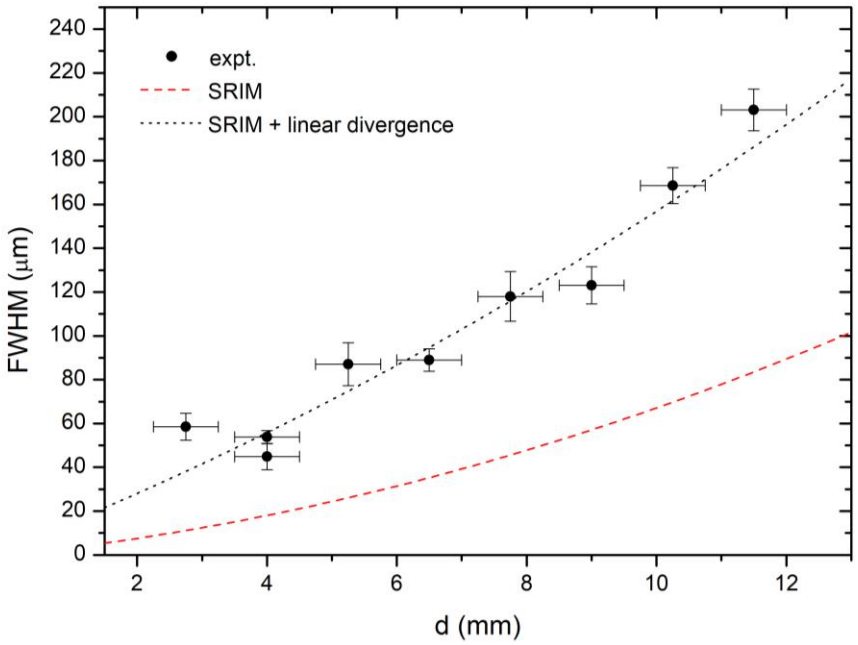


**Figure 3:** Measured lateral dimension of the proton beam expressed as FWHM as a function of the distance from the exit window. Error bars represent the fitting errors.

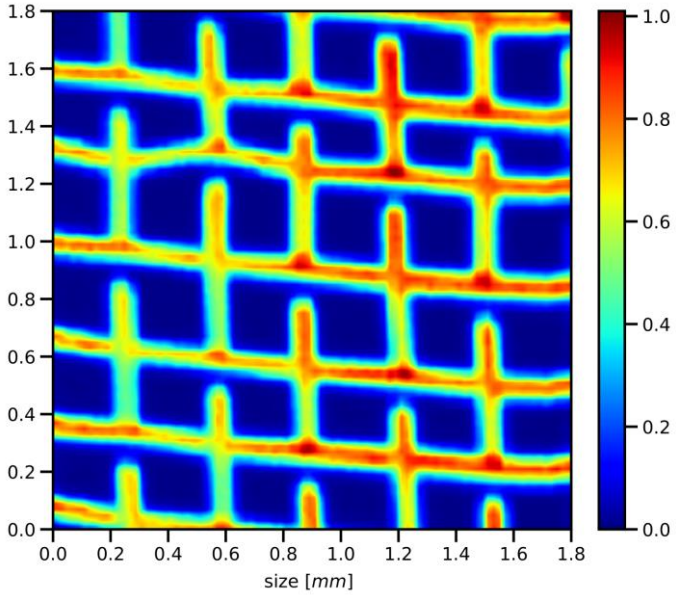


**Figure 4:** Measured PIXE map of a Platinum/Rhodium mesh (Pt90/Rh10) mesh. The map is composed of 90×90 points, the acquisition time per single point was 3 s.

Another very important part of the upgrade is the beam chopper used to determine the proton dose deposited on the sample, which is necessary to perform quantitative analysis. After the installation we have tested the stability and accuracy of the proton dose measurement by observing the ratio of the X-ray yield recorded from a homogeneous Ni metallic target and the Au RBS yield from the chopper. The ratio was found very stable, the values measured within first 5000 s are presented in Figure 5. The

standard deviation of the measured yield ratio was found 1.4% which is consistent with the statistical error of the measured RBS yield.

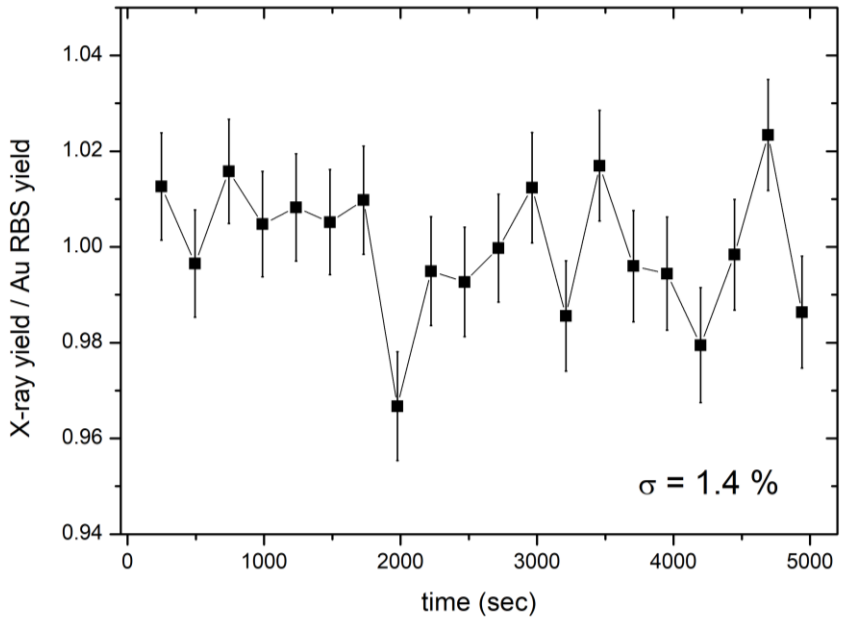


**Figure 5:** Measured ratios of the integrated K X-ray yield from Ni metallic target and Au RBS yield from the chopper.

In order to finally perform full quantitative PIXE analysis we need to calibrate the proton dose measurement together with the efficiency and solid angle of the X-ray detector. This calibration was done by measuring a set of K X-ray spectra from several mono-elemental homogeneous thick samples. The absolute calibration factor between the proton dose and the Au RBS chopper yield was determined by analyzing the measured PIXE spectra with the GeoPIXEII software package [13]. This calibration factor was found 3.5 $10^{-2}$ nC/count yielding the overall beam chopper sensitivity of approximately 0.3 cts/sec within RBS signal per pA proton current on the sample. Standard deviation of the calibration factor measured for different calibration targets was found 5.4% and this value was assigned as the final experimental uncertainty. After this calibration, absolute quantitative in-air PIXE analysis can be performed without using any reference material. However, just to check all experimental parameters and confirm the reliability of the overall quantification procedure a PIXE spectrum from reference material is recorded before every experimental run. Generally, any external reference standard could be used but we usually try to use a material of composition similar to the studied sample. Finally, the calibration procedure was checked by measuring two standard reference materials from National Institute of Standards and Technology (NIST), NIST 1107 (naval brass) and NIST 1573a (tomato leaves) and analyzing the measured spectra with the GeoPIXE. The measured concentrations are presented in Table 1 and 2, quoted uncertainties include also the calibration uncertainty described before. With the exception of calcium in NIST 1573a, all measured concentrations are within experimental uncertainties in agreement with certified values.

| Naval brass NIST | Measured values | Certified values |
|---|---|---|
| Cu | 62.6±3.4% | 61.183±0.074% |
| Zn | 37.8±2.0% | 37.396±0.084% |
| Sn | 0.90±0.07% | 1.066±0.015% |
| Ni | 880±120 ppm | 950±40 ppm |
| Fe | 699±180 ppm | 390±30 ppm |

**Table 1.** Absolute concentrations of several major and minor elements within NIST 1107 standard reference material determined by in-air PIXE analysis. Measured concentrations are compared with certified values.

| NIST 1573a | Measured values | Certified values |
|---|---|---|
| K | 2.53±0.14 % | 2.676±0.048 % |
| Ca | 3.93±0.21 % | 5.045±0.055 % |
| Mn | 256±16 ppm | 246±7 ppm |
| Fe | 380±23 ppm | 368±4 ppm |
| Cu | 6±3 ppm | 4.7±0.14 ppm |
| Zn | 32±4 ppm | 30.9±0.6 ppm |

**Table 2.** Absolute concentrations of several major and minor elements within NIST 1573a standard reference material determined by in-air PIXE analysis. Measured concentrations are compared with certified values.

## III. FIRST APLICATION

Mineral deficiency is a widespread nutritional disorder especially prevalent in developing countries with a cereal dominant diet [14,15]. Mineral nutrients (Mg, S, P, K, Ca, Fe, Zn) are present in cereals but are unevenly distributed across the grains with the highest accumulation in tissues which are generally removed in the grain processing for the human consumption (seed coat, aleurone layer and embryo). Since understanding the localization and accumulation of elements in plants is an important topic in a range of fields, different techniques have been used for analysis of biological samples [16]. Elemental distribution patterns among different grain genotypes can be distinguished using micro-PIXE technique which provides precise localization of minerals and their accumulation levels. Therefore, the investigation of mineral co-localization and nutrient transport in different grain tissues is crucial for nutritional improvement of grain crops and selection of the appropriate genotypes. While the elemental distribution in wheat grain tissues was previously examined by in-vacuum micro-PIXE [17,18], micro-PIXE in ambient atmosphere enables analysis of thick samples and whole plant organs (leaf, root, grain etc.) and hydrated biological specimens with minimal sample preparation.

The first application of the updated external beam was the micro-PIXE mapping of a thick longitudinal section of a wheat grain in ambient environment. The morphology of the grain as seen under the optical microscope is presented in Figure 6. A 3 MeV proton beam was used in these measurements, the sample distance from the exit nozzle was 3 mm and the overall scanning area was

3.3 × 7.8 $mm^2$. The X-ray detector was positioned 3 cm from the target to attain a solid angle of about 0.022 sr; in order to stop scattered proton to reach the detector crystal it was equipped with a 100 μm kapton absorber. Mapping was performed by mechanical scanning using a dedicated home-made software written in the LabVIEW programming environment which controls the positioning stage and reads consecutive PIXE spectra from the XiA DPP used to process the signal from X-ray detectors. The acquisition time for single point was 3 s. During PIXE mapping, RBS spectra from the chopper was simultaneously recorded in parallel with PIXE spectra and used to determine quantitatively final concentrations and also to normalize separate points in the map due to possible fluctuations of the proton beam intensity. Since the RBS signal from the chopper is too weak to provide statistically high enough

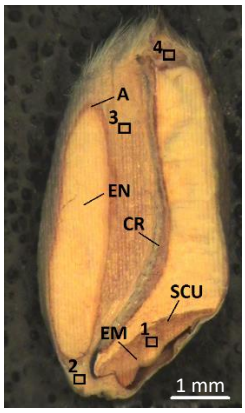


**Figure 6:** Morphological structures of a thick longitudinal section of wheat grain as seen in optical microscope image with different regions of the grain marked as AL-aleurone layer, EM-embryo, CR-crease, SCU- scutellum and EN-endosperm. The individual areas used for average tissue elemental concentration evaluation are marked.

signal from each separate measuring point the Au RBS signal is integrated every 250 seconds and linear interpolation of the neighboring points is used for normalization and dose determination of each measured PIXE spectrum. Measured PIXE spectra were analyzed using GeoPIXE software package. The final quantitative elemental distribution maps are presented in Figure 7. Due to in air X-ray absorption, some of the elements which are common in plant tissues (Na, Mg, P, S), were below the detection limit of in-air micro-PIXE. The elemental distribution maps indicate that K is predominant element in the grain, mainly present in aleurone layer, embryo and scutellum. Fe and Zn seem to co-localize in the aleurone layer and embryo with varying concentrations. Mn was predominantly measured along the crease of the grain while Ca was present in the whole grain with higher concentrations measured around the pigment strand and in 'hotspots' within the endosperm. Finally, we have also calculated average section-specific concentrations for four 5×5 pixel sub regions (300 x 300 $\mu m^2$) using GeoPIXE and these are tabulated in Table 3.

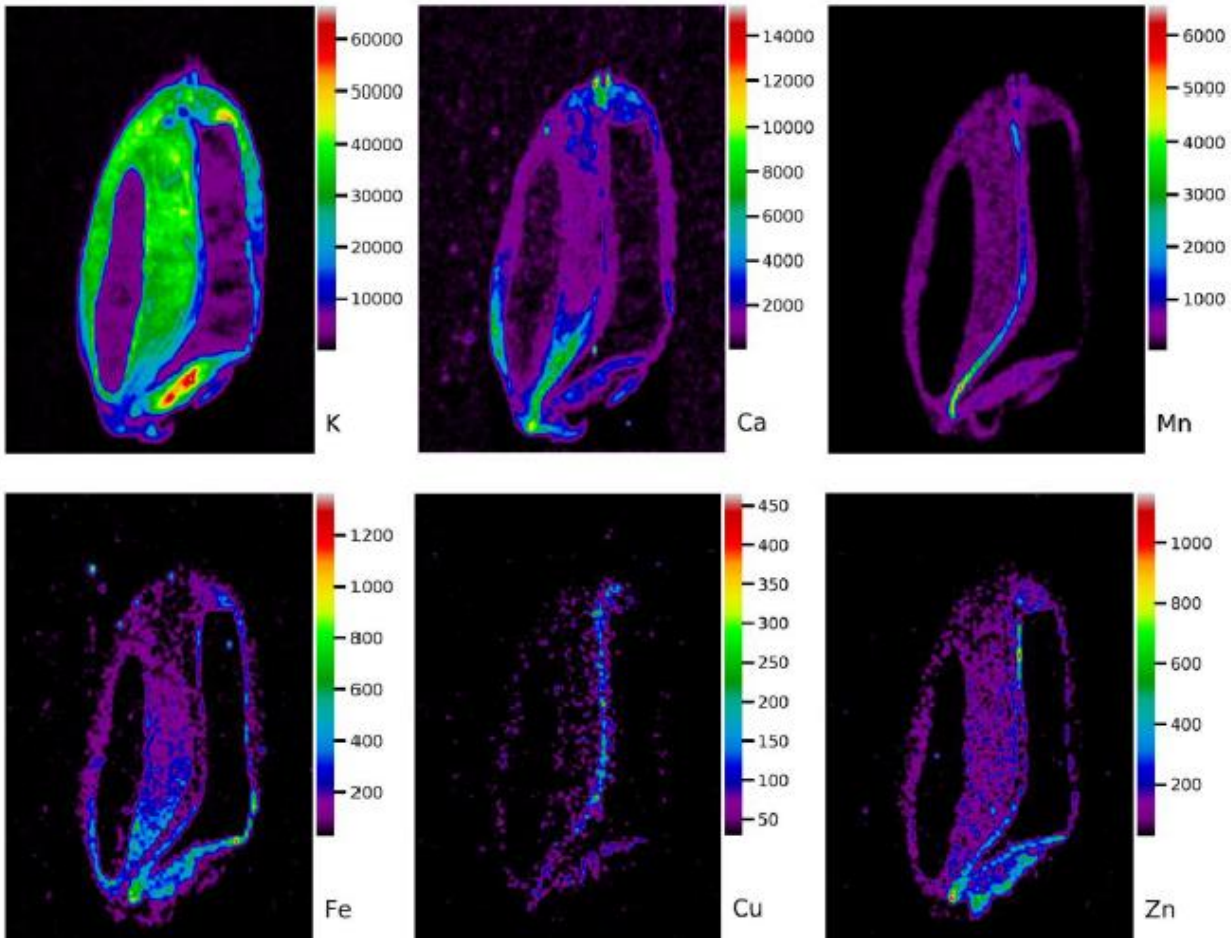


**Figure 7:** Elemental distribution maps of elements in wheat grain, concentrations are presented in ppm. Total scanning area was 55 × 130 pixels with a 60 μm step and 3 s acquisition time per point.

Next, we zoomed in on embryo region of the grain and performed another more detailed scan with 20 μm step size over smaller area (2.4 × 1.7 $mm^2$). Mapping with a smaller step size allowed for a more precise localization of higher concentrations of specific elements in the region. Generally, the final lateral resolution is limited by the size of the proton beam and this defines the smallest scanning step used in the PIXE imaging. However, in case of smaller scan area we can apply also smaller step since approximately 100×100 pixels are required to build an image. The resolution is not enhanced but we acquire larger statistics over smaller area yielding more accurate average concentrations in specific sub regions.

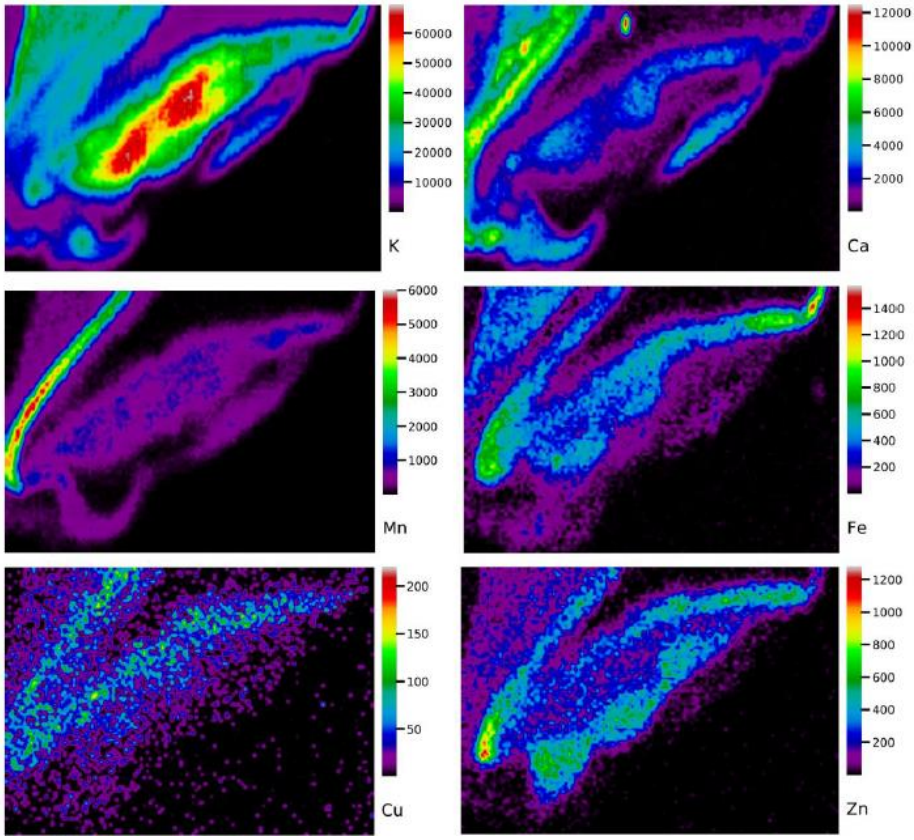


**Figure 8:** Elemental distribution maps of elements on a zoomed in area of wheat grain, concentrations are presented in ppm. Scan size was 120×85 pixels with a 20 μm step and 3 s acquisition time per point.

| | K [%] | Ca [%] | Mn [ppm] | Fe [ppm] | Cu [ppm] | Zn [ppm] |
|---|---|---|---|---|---|---|
| Area 1 | 4.25±0.032 | 0.21±0.005 | 571±19 | 330±12 | 33±7 | 218±18 |
| Area 2 | 1.41±0.006 | 0.448±0.002 | 1368±4 | 235±3 | 31±5 | 109±6 |
| Area 3 | 2.026±0.02 | 0.067±0.004 | 190±10 | 71±7 | <lod | 41±8 |
| Area 4 | 2.36±0.017 | 0.268±0.004 | 198±11 | 110±7 | <lod | 67±9 |

**Table 3:** Average concentrations of elements in selected areas of the wheat grain. Area numbers correspond to square numbers on Figure 6.

The elemental distribution maps gave us an overall image of localization of minerals in the whole grain and, with lateral resolution of 50 μm, we were able to distinguish different regions of the wheat grain such as aleurone layer which has an average thickness of 30-70 μm [19]. The average concentrations of measured elements are in agreement with those previously reported [17, 18] with the exception of Mn. The high concentration of Mn is potentially due to slicing of the grain right through the pigment strand where Mn is primarily accumulated. Therefore, we conclude that in-air micro-PIXE can be used as a complementary method to in-vacuum micro-PIXE analysis of biological samples.

## IV. CONCLUSIONS

In this paper the upgrade and the current status of the external proton microbeam at the Microanalytical Center of the Jožef Stefan Institute are presented. The new setup can be used to perform in-air PIXE mapping with ~ 50 μm lateral resolution. This was achieved by focusing the proton beam with a doublet of magnetic quadrupole lenses and replacing the previous exit window with a 200 nm $Si_3N_4$ foil. The deposited proton dose used for quantification is measured with the in-beam chopper device. The performance and experimental capability of the new setup are demonstrated with an example of full quantitative PIXE imaging of an entire thick longitudinal cut of wheat grain and a zoom in on the embryo region. Future steps include the use of He flow to allow detection of lighter elements and the installation of the parallel beam wavelength dispersive (PB-WDS) X-ray spectrometer which will enable high energy resolution PIXE measurements and spread the analytical capability of the external beam setup even further.

## ACKNOWLEDGEMENTS:

This work was supported by the RADIATE project under the Grant Agreement 824096 from the EU Research and Innovation programme HORIZON 2020 and by the Slovenian Research Agency through the research program P1-0112.

**References:**

[1] J. Simičič, P. Pelicon, M. Budnar, Ž. Šmit, Nucl. Instrum. Methods B 190, 2002, 283-286.

[2] P. Pongrac, R. Tolra, R. Hajiboland, K. Vogel-Mikuš, M. Kelemen, P. Vavpetič, P. Pelicon, J.Barceló, M. Regvar, C. Poschenrieder, Food and Chemical Toxicology 135 (2020), p.110974.

[3] P. Pongrac, H. Castillo-Michel, J. Reyes-Herrera, R. D. Hancock, S. Fischer, M. Kelemen, A. J. Thompson, G. Wright, M. Likar, R. M. Broadley, P. Vavpetič, P. Pelicon & J. P. White, BMC Plant Biol 20 (2020), 368.

[4] E. Punzón-Quijorna, M. Kelemen, P. Vavpetič, R. Kavalar, P. Pelicon, K. S. Fokter, Nucl. Instrum. Methods B, 462 (2020), 182-186.

[5] M. Budnar, J. Simčič, Z. Rupnik, M. Uršič, P. Pelicon, J. Kolar, M. Strlič, Nucl. Instrum. Methods B, 219–220 (2004), 41-47.

[6] D. Jezeršek, Ž. Šmit, P. Pelicon, Nucl. Instrum. Methods B, 268 (2010), 2006.

[7] Ž. Šmit, B. Maroti, Z. Kasztovszky, A. Semrov, P. Kos, Archaeological and Anthropological Sciences 12, (2020), p.81.

[8] Ž. Šmit, A. Semrov, Nucl. Instrum. Methods B 100 (2018), p.10415.

[9] N. Piel, M. Berheide, Ch.Polaczyk, C.Rolfs, W.H.Schulte, Nucl. Instrum. Methods A, 349, (1994), p.18-26.

[10] M. Massi, L. Giuntini, M. Chiari, N. Gelli, P. A. Mandò, Nucl. Instrum. Methods B, 190, 1–4, (2002), p.276-282.

[11] D. Wright, P. Greve, J. Fleischer, and L. Austin, Opt. Quantum Electron. 24, S993–S1000 (1992).

[12] T. Calligaro, J.-C. Dran, E. Ioannidou, B. Moignard, L. Pichon, J. Salomon, Development of an external beam nuclear microprobe on the Aglae facility of the Louvre museum, Nucl. Instrum. Methods B, 161–163, 2000, 328-333.

[13] C. G.Ryan, Int. J. Imaging Syst. Technol. 11, (2000), p.219–230.

[14] B. R. Singh, Y. N. Timsina, O. C. Lind, S. Cagno, K. Janssens, Zinc and Iron Concentration as Affected by Nitrogen Fertilization and Their Localization in Wheat Grain, Front. Plant Sci. 9, 2018, 307.

[15] K. L. Moore, F.-J. Zhao, C. Gritsch, P. Tosi, M. Hawkesford, S. Mcgrath, P. Shewry, C. R. M. Grovenor, Journal of Cereal Science 55, 2012, 1836.

[16] P. M. Kopittke, E. Lombi, Avan der Ent, et al., Plant Physiol. 182(4),(2020), p.1869-1882.

[17] P. Pongrac, I. Kreft, K. Vogel-Mikuš, M. Regvar, M. Germ, P. Vavpetič, N. Grlj, L. Jeromel, D. Eichert, B. Budic et al., Journal of the Royal Society Interface 10, (2013),p.20130296.

[18] P. S. Sudhir, K. Vogel-Mikuš, P. Vavpetič, L. Jeromel, P. Pelicon, J. Kumar, R. Tuli, Planta 240, (2014), p.277.

[19] D. B. Bechtel, J. Abecassis, P. R. Shewry, A. D. Evers, CHAPTER 3 - Development, Structure, and Mechanical Properties of the Wheat Grain, Editor(s): Khalil Khan, Peter R. Shewry, In American

Associate of Cereal Chemists International, Wheat (Fourth Edition), AACC International Press, 2009, Pages 51-95.